SCIEPublish

Review

Mini Review on the Photocatalytic Removal of Gaseous Ammonia: Current Status and Challenges

Yanxu Wang, Yang You, Yuhan Guo and Shaojun Yuan *

Low-Carbon Technology & Chemical Reaction Engineering Lab, College of Chemical Engineering, Sichuan University, Chengdu 610065, China; yxwscu@163.com (Y.W.); 15983556540@163.com (Y.Y.); 17882705322@163.com (Y.G.)

* Corresponding author. E−mail: ysj@scu.edu.cn (S.Y.); Tel./Fax: +86-28-85405201 (S.Y.)

Received: 3 December 2024; Accepted: 25 December 2024; Available online: 30 December 2024

ABSTRACT: Ammonia gas (NH_3) is a notorious malodorous pollutant released mainly in agriculture and industry. With the increasing demand for ammonia, environmental pollution caused by ammonia discharge has seriously threatened human health and safety. Due to the discrete emission and low concentration of NH_3, photocatalytic oxidation is an economical and efficient treatment strategy. TiO_2, as a common photocatalyst, has been widely used by researchers for the photocatalytic removal of NH_3. In addition, surface modification, element doping, semiconductor recombination and metal loading are used to improve the utilization rate of solar energy and carrier of TiO_2 so as to find a catalyst with high efficiency and high N_2 selectivity. Further, at present, there are three main removal mechanisms of NH_3 photocatalytic oxidation: $\cdot NH_2$ mechanism, iSCR mechanism and N_2H_4 mechanism. Among them, N_2H_4 mechanism is expected to be the main removal path of NH_3 photocatalytic oxidation in the future because the removal process does not involve NO_x and nitrate. This review summarizes recent studies on the photocatalytic oxidation of NH_3, focusing primarily on NH_3 removal efficiency, N_2 selectivity, and the underlying removal mechanisms. Additionally, the potential future applications of NH_3 photocatalytic oxidation are discussed.

Keywords: Gaseous ammonia; Photocatalytic oxidation; NH_3 removal; Reaction mechanism

1. Introduction

As early as the 18th century, ammonia was used in agricultural production as a fertilizer. At present, the global annual production of nearly 200 million tons of ammonia is mainly used in agriculture and industry, and the demand is increasing year by year. Recently, ammonia is also used directly as a fuel or good carrier for hydrogen because its energy density is similar to fossil fuels and more stable than hydrogen energy. For example, the emergence of technologies such as ammonia fuel engines and NH_3 fuel cells highlights the significant potential of ammonia as a clean chemical energy source, thereby contributing to the achievement of carbon neutrality objectives [1–4]. However, with the increase in ammonia demand and application range, the environmental pollution caused by ammonia has become an urgent problem to be solved. Ammonia gas (NH_3) is a hazardous and malodorous pollutant released in substantial quantities from various sources [5,6], including agriculture [7,8], composting centers [9], municipal biowaste [10–12], vehicle exhaust [13–16], and fossil fuel combustion [17]. NH_3 reacts with acidic gases in the air (such as NO_x and SO_2) to form particulate matter with a diameter of less than 2.5 μm (PM2.5) [18,19]. What's more, NH_3 can generate secondary aerogel to promote the formation of haze and photochemical smog, causing serious pollution to the global atmospheric environment [5]. Recent studies have shown that NH_3 emissions (25–39%) contributed more to PM2.5 than NO_x emissions (23–33%) globally in 2013 and suggest that controlling NH_3 emissions is much cheaper than controlling NO_x emissions [20]. Moreover, NH_3 can irritate the human eye and respiratory organs and can be fatal in high concentrations, posing a serious threat to public health and safety. In order to protect people's health, countries all over the world have strict regulations on NH_3 emissions. For example, the Occupational Safety and Health Administration sets the maximum exposure limit for NH_3 at 25 ppm for 8 h and the short-term exposure limit at 35 ppm for 15 min. That of the China Emission Standard for Odor Pollutants is less than 0.2 mg/m^3 (0.15 ppm). In addition, the researchers show that the cost

https://doi.org/10.70322/gct.2024.10010

of reducing NH_3 emissions is only 10% of the cost associated with controlling NO_x emissions, suggesting that managing NH_3 emissions can be a more economical approach to reducing both NO_x and PM2.5 emissions. If global NH_3 emissions are reduced by 50%, the implementation cost will be around $38 billion. This is significantly lower than the estimated social benefits of preventing deaths linked to NH_3 emissions and their contribution to PM2.5 pollution, which total $172 billion [20]. Furthermore, the researchers further emphasize the priority of European policies aimed at controlling NH_3 emissions. For each unit of PM2.5 control, the cost−effectiveness of reducing NH_3 emissions is 5 to 11 times greater than that of reducing NO_x. Moreover, the impact of NH_3 reduction on nitrate and ammonium nitrogen levels is pronounced, with average annual sensitivities of 81.9% and 34.8%, respectively [21]. Consequently, it is urgent to solve the NH_3 problem directly at the point source [6].

At present, NH_3 emission has the characteristics of discrete emission, and the concentration is mostly ppm level. Conventional treatment strategies for NH_3 are divided into physical, biological and chemical methods. The physical methods include adsorption, absorption and condensation. Among them, the absorption and condensation methods are suitable for the treatment of high-concentration NH_3, but the equipment and operation costs are huge [22,23]. The adsorption method is suitable for the treatment of low and medium-concentrations of NH_3, but the change in the adsorbent and desorption process increases its cost [24,25]. The biological method also has the disadvantages of poor removal efficiency and large equipment footprint, and the culture and replacement of bacterial organisms will also cause huge costs [26,27]. In addition, thermal catalytic oxidation in chemical methods needs to be carried out at a higher temperature [28–31]. In contrast, photocatalytic oxidation has mild processing conditions and simplified equipment operation, providing a cost-effective and environmentally friendly route for NH_3 removal. Furthermore, this method has demonstrated tremendous potential in treating various gaseous pollutants, such as the removal of volatile organic compounds, purification of indoor formaldehyde, and reduction of NO_x emissions [32,33]. Therefore, it is very promising to remove NH_3 by direct photocatalytic oxidation to N_2 and H_2O at the point source. The design of efficient photocatalysts for NH_3 oxidation, capable of achieving high activity in NH_3 conversion while minimizing the formation of by-products such as NO_x and N_2O, represents one of the core challenges in this field. In this case, it is necessary to select an economical and efficient photocatalyst with high nitrogen selectivity. As a common photocatalyst, TiO_2 has been widely used in the photocatalytic removal of NH_3. Under the irradiation of light, the electrons in the valence band (VB) of TiO_2 are excited to transition to the conduction band (CB) and form a photogenerated carrier (electron-hole pair). Subsequently, part of the photogenerated charge carriers (e^- and h^+) migrated to the surface of TiO_2 and reacted with the adsorbed substances on the surface or produced active substances ($\cdot O_2^-$ and $\cdot OH$) [34]. The active substance will also be further involved in the chemical reaction, thus oxidizing the NH_3 to N_2 and H_2O. However, the application of TiO_2 is restricted by its wide band gap width and low carrier utilization [34–36]. To address these limitations, the researchers have employed strategies such as surface modification, metal loading, doping modification, and semiconductor compositing to enhance the utilization of solar energy and carriers in TiO_2 [37–40]. Additionally, the impact of different modification strategies on the photocatalytic activity of catalysts and the mechanism of NH_3 removal is still not clear.

In this review, we aim to provide guidance for the development of NH_3 photocatalytic oxidation systems. Relevant researches on photocatalytic oxidation of NH_3 in recent years are analyzed, with a focus on photocatalytic oxidation performance, carrier and solar energy utilization efficiency, as well as the oxidation pathway of NH_3. The purpose of this paper is to clarify the difficulties and challenges existing in the current photocatalytic oxidation of NH_3, and put forward our views on improving the photocatalytic efficiency of NH_3, so as to provide new ideas and guidance for the removal of environmental pollutants.

2. Catalyst for Photocatalytic Oxidation of NH_3

2.1. TiO_2 Based Photocatalyst

TiO_2 has emerged as an advanced photocatalyst for tackling environmental pollution due to its eco-friendliness, low cost, renewability, and high photocatalytic activity. However, the wide bandgap of TiO_2 results in low efficiency in utilizing visible light and significant carrier recombination, which leads to suboptimal photocatalytic performance [34]. Nevertheless, a range of modification techniques, such as doping with metal or non-metal ions, loading metal co-catalysts, and constructing heterostructured semiconductor catalysts, can greatly improve its efficiency in visible light utilization and carrier separation. In this section, we first studied the application of TiO_2-based photocatalyst in the photocatalytic oxidation of NH_3.

2.1.1. Pure TiO_2 Photocatalyst

TiO_2 has three common crystal structures, among which anatase and rutile are the two most studied polymorphs. The bandgap width of rutile is approximately 3.0 eV, while that of anatase is about 3.2 eV. From the perspective of bandgap width, rutile TiO_2 has a narrower bandgap, which implies a broader range of light absorption [41]. However, the recombination of charge carriers in rutile TiO_2 is more severe, resulting in its photocatalytic ability being inferior to that of anatase TiO_2. Additionally, anatase TiO_2 has a stronger hydroxyl acidity on its surface, leading to a greater adsorption capacity for NH_3 molecules. Wu et al. prepared a modified TiO_2 catalyst using the sol−gel method and tested it under visible and ultraviolet light (Figure 1a). The results showed that the TiO_2 catalyst calcined at 400 °C exhibited the best ultraviolet light activity with a conversion rate of approximately 43%. Their study found that surface acidic sites play a crucial role in NH_3 PCO. As the calcination temperature increased, the specific surface area and pore volume of the TiO_2 samples gradually decreased. However, the sample calcined at 400 °C still maintained a relatively high specific surface area (145.2 m^2/g) and good crystallinity. The high specific surface area and good crystallinity are conducive to forming more acidic sites. Additionally, after high-temperature calcination, surface carbon impurities were reduced, thereby preserving more acidic sites [42].

Although anatase offers distinct advantages, TiO_2 containing both anatase and rutile phases (such as P25) is widely used in various catalytic reactions. Heylen et al. show that the conversion efficiency of commercial P25 for NH_3 at 150 °C is only 60%, primarily yielding by-products like NO and NO_2, with an N_2 selectivity of merely 28%. Even when the space velocity is reduced by half, the selectivity of P25 does not significantly improve. In contrast, the PC500 TiO_2 catalyst achieves a 99% conversion rate and 92% dinitrogen selectivity under conditions of 150 °C, 300 VHSV h^{-1}, and 1.1 mW/cm^2 UVA irradiation. Compared to P25 and UV100, PC500 exhibits greater weight loss (approximately 12%) in thermogravimetric analysis (TGA), indicating a higher water adsorption capacity on its surface, which may enhance its NH_3 adsorption capability. At lower temperatures (100 and 50 °C), the NH_3 conversion rate of PC500 decreases, but the selectivity for NO increases, suggesting the potential involvement of an internal selective catalytic reduction (iSCR) mechanism [43]. In addition, Sola et al. compared the differences in the gas-phase photocatalytic degradation of NH_3 and ethanol on two commercial TiO_2 materials (Evonik's P25 and Sigma Aldrich (SA)) in the presence of water. The photodegradation process was tracked using FTIR to analyze changes over irradiation time. The research found that during the NH_3 photodegradation process, surface nitrate species remained firmly bound on P25, while they were eliminated on SA. This was attributed to the presence of more and stronger Lewis acid sites on the SA surface, as well as a greater number of reactive surface hydroxyl species. The adsorbed NH_3 could react with the generated nitrate species to form N_2, a reaction mechanism that was lacking on the P25 surface (Figure 1b) [44]. In summary, for pure TiO_2 photocatalysts, the anatase phase seems to be more suitable for the photocatalytic oxidation of NH_3 because of its better removal performance and N_2 selectivity than the rutile phase.

In addition, the main exposed crystal plane of anatase TiO_2 is the (1 0 1) crystal plane because its average surface free energy (0.44 J/m^2) is lower than that of the (0 0 1) crystal plane (0.90 J/m^2). However, He et al. prepared TiO_2 with the main exposure surface of (0 0 1) crystal plane by surface fluoridation with HF acid and found that it had better performance for the photocatalytic oxidation of NH_3. The experimental results (Figure 1c) show that the ≡Ti−F group on the surface of the photocatalyst can delay the recombination of photogenerated e^- and h^+, which may be the main reason for the excellent activity of F−TiO_2 catalyst [45]. Further, using H_2O and NH_3 photooxidation as probe reactions, they investigated the effect of surface F ions on carrier migration in anatase TiO_2 crystals dominated by (0 0 1) or (1 0 1) planes. Fluorinated (F-T001) and defluorinated (T001) TiO_2 with exposed (001) crystal faces and TiO_2 with exposed (1 0 1) crystal faces (T101) and fluorinated (1 0 1) (T101-F) and (0 0 1) (T001-F) crystal faces are synthesized. They observed a significant synergistic effect of the (0 0 1) plane and surface F ions on photogenic hole migration. The (0 0 1) plane provides h^+ trapping sites, and the electrostatic effect of surface F ions attracts and accelerates the migration of h^+ to the (0 0 1) plane and collaboratively promotes the separation of electron-hole pairs, thus significantly improving the photooxidation activity (Figure 1d). However, there is no synergy between the (1 0 1) plane and the surface F ions [46]. Furthermore, they prepared anatase TiO_2 with (0 0 1), (1 0 1) and (0 1 0) clean dominant planes (denoted as T001, T101 and T010) and tested their photocatalytic activity for NH_3 oxidation. The results (Figure 1e) showed that the order of photocatalytic activity of NH_3 oxidation is (0 0 1) > (1 0 1) > (0 1 0). This is due to the special effect of the (0 0 1) crystal plane on the h^+, which can promote the transition of NH_3 molecules to·NH_2 [47].

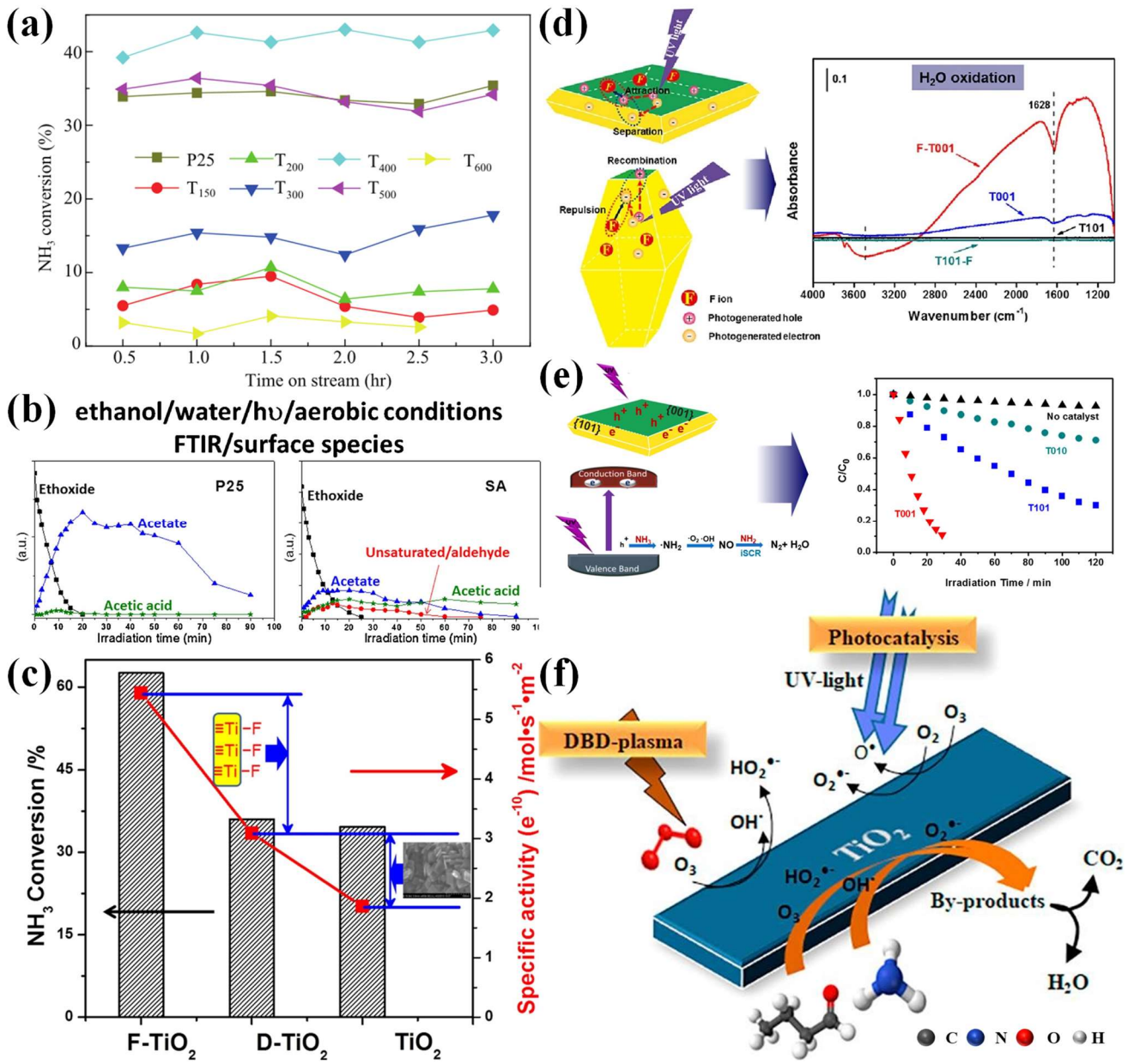

Figure 1. (**a**) NH_3 photocatalytic oxidation of TiO_2 at different calcination temperatures [42]. (**b**) The variation of different species on P25 and anatase TiO_2 over time [44]. (**c**) The photocatalytic oxidation of NH_3 on surface-fated TiO_2 ($F{-}TiO_2$), defluorinated TiO_2 ($D{-}TiO_2$) and pure TiO_2 [45]. (**d**) IR spectra of F-T001, T001, T001-F, T101-F and T101 after 5 min UV irradiation under N_2 atmosphere [46]. (**e**) The photocatalytic oxidation of NH_3 on T010, T101 and T001 [47]. (**f**) Synergistic removal of NH_3 and butyraldehyde by DBD and photocatalytic oxidation on TiO_2 [48]. Reproduced with permission. Copyright 2014, 2016, 2017 and 2018, Elsevier Publication.

Several studies have investigated the efficacy of TiO_2 photocatalysis in the removal of NH_3 from mixed gas pollutants under practical conditions. Research conducted by Saoud et al. demonstrates that when pollutants are treated individually, the removal efficiency for the removal of NH_3 is 15%, while that for butanal is 45%. However, when both pollutants are treated simultaneously, the removal efficiency for NH_3 decreases to 12%, and for butanal, it decreases to 33%. This reduction in photocatalytic oxidation efficiency is likely due to the competitive adsorption of the two pollutants on the active sites. In contrast, dielectric barrier discharge (DBD) plasma exhibits a higher degradation efficiency for ammonia (Figure 1f). Under specific energy input (SEI) conditions, DBD plasma alone achieves a removal efficiency of 51%. Furthermore, coupling DBD plasma with photocatalytic oxidation significantly enhances the removal efficiency for ammonia, achieving a rate of 83%, indicating a synergistic interaction between the two methods [48].

2.1.2. Doped Modified TiO_2 Photocatalyst

Doping modification is mainly divided into metal element doping (Fe, Cu, Ce, *etc.*), non-metallic element doping (N, S, C, *etc.*) and metal and non-metallic element co-doping. For the photocatalytic oxidation of ammonia, doping modification mainly contributes to three aspects. (i) The formation of oxygen vacancy (Ov). On the one hand, Ov, as a Lewis acidic site, can promote the adsorption of NH_3. On the other hand, Ov can also be used as e^-−h^+ traps to promote the separation of photogenerated carriers and enhance photocatalytic activity. (ii) As an e^-−h^+ trap. Similar to the role of Ov, the introduced ions can also act as electron or hole traps, thereby improving carrier utilization. (iii) Broaden the optical response range. The introduced elements can form impurity levels below the CB or above the VB of the photocatalytic semiconductor, thereby reducing the band gap (E_g) width of the photocatalyst and broadening the light absorption range. However, a significant drawback of doping is that the introduction of heteroatoms, whether through atomic substitution or occupancy of interstitial sites, inevitably alters the atomic structure of the photocatalyst and may lead to the formation of recombination centers [49]. Excessive doping can diminish catalytic performance by modifying the atomic structure and creating additional recombination sites. Therefore, precise optimization of the doping ratio is essential for effective modification of the photocatalyst.

Wang et al. prepared Fe-doped TiO_2 (Fe−TiO_2) thin films by sol−gel method (Figure 2a) to degrade typical indoor air pollutants HCHO, NH_3 and C_6H_6 under sunlight irradiation, and the removal efficiency of NH_3 was 53.1% after 9 h. By replacing Ti^{4+} ion, Fe^{3+} ion introduced a new impurity energy level between the CB and the VB, which decreased the E_g and inhibited the e^-−h^+ pair recombination and improved the photocatalytic activity [50]. In addition, the researchers prepared 5% N/Ag−TiO_2 by in-situ solvothermal method, which showed 4.3 times higher photocatalytic performance than pure TiO_2. The introduction of Ag ions formed an impurity energy level below the CB, which significantly reduced the band gap energy of TiO_2 from 3.2 to 1.7 eV and increased the absorption of visible light (Figure 2b). At the same time, Ag ion acted as an e^- trapping site and slowed down the recombination of carriers. N doping increases the specific surface area of the catalyst and enhances the NH_3 adsorption [51]. Similarly, Wang et al. synthesized Mo, C−TiO_2 photocatalyst by sol−gel synthesis and low-temperature calcination using organic groups in TiO_2 precursor as a carbon source. Experimental results demonstrated that the incorporation of carbon extended the photo-response range of TiO_2, while the inclusion of Mo was found to effectively suppress the recombination of photogenerated carriers under both UV and visible light conditions (Figure 2c). The co-doping of Mo and C further facilitated the formation of Ov, thereby improving the photocatalytic oxidation performance under both UV and visible light irradiation. Meanwhile, in their proposed N_2H_4 mechanism, Mo ions served as the reactive active site, and NH_3 adsorbed on it reacted with the reactive oxygen species gradually to generate N_2 as the expected end product [52].

In addition, non-metallic elements (such as C, N) are also used to improve the photocatalytic NH_3 removal performance of TiO_2. Using urea as the N source, Jiang et al. prepared N−TiO_2 and used it for NH_3 removal under visible light. The results show (Figure 2d) that the efficiency of N−TiO_2 photocatalytic oxidation of NH_3 remains above 80%, and the N_2 selectivity is stable at about 87%. In contrast, the NH_3 conversion on pure TiO_2 stabilized at about 67% within 72 h, and the nitrogen selectivity did not exceed 55%. N element was successfully doped into the TiO_2 lattice system in the form of O−Ti−N, which reduced the band gap energy from 3.18 to 3.07 eV, improving the light utilization rate. Secondly, the water molecules formed during the reaction contribute to the continuous formation of hydroxyl radical (·OH) in the in-situ reaction, thus improving the stability of the reaction [53]. Further, Gao et al. added a carbon layer to N−TiO_2 and tested the activity of NH_3 photocatalytic oxidation under visible light (Figure 2e). The results show that the ammonia removal efficiency and N_2 selectivity of C/N−TiO_2 catalyst is 94% and 98%, respectively. The co-doping of C and N reduces the band gap of TiO_2 (3.18~2.90 eV), thus broadening the photo-response range of TiO_2. At the same time, more Ov was formed under visible light irradiation, which improved the activity of the catalyst. Additionally, more acidic sites were introduced, which improved the adsorption capacity of the catalyst for NH_3 [54].

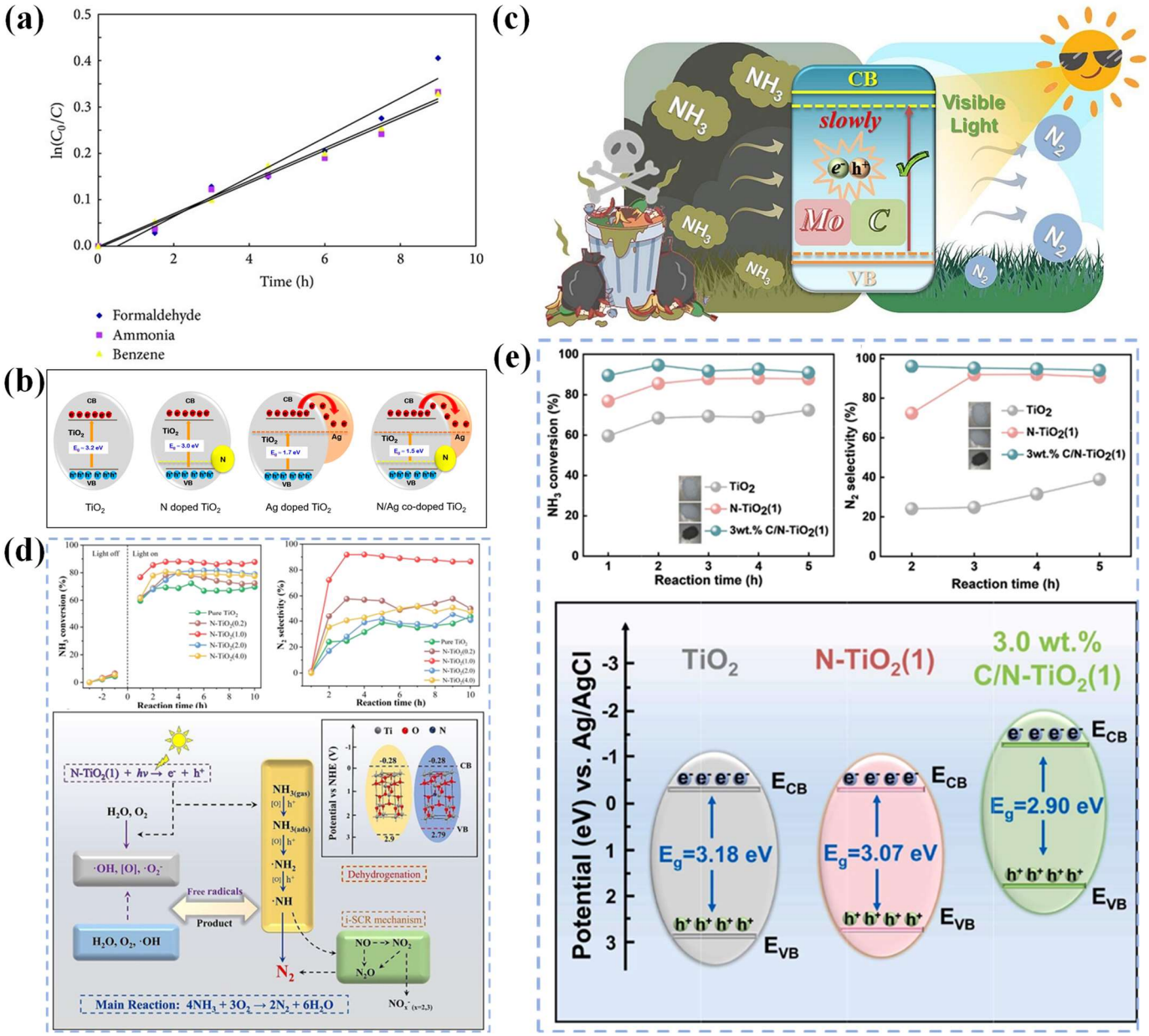

Figure 2. (**a**) Kinetics of degradation reaction of the mixed pollutants on Fe−TiO_2 [50]. Reproduced with permission. Copyright 2014, WILEY Publication. (**b**) Schematic diagrams of the band energy structure and the migration of photoexcited electrons in undoped TiO_2, N−TiO_2, Ag−TiO_2, and N/Ag−TiO_2 [51]. Reproduced with permission. Copyright 2020, MDPI Publication. (**c**) Schematic diagram of photocatalytic oxidation of NH_3 on Mo, C−TiO_2 [52]. (**d**,**e**) Photocatalytic oxidation of NH_3 on N−TiO_2, C/N−TiO_2 and pure TiO_2 under visible light [53,54]. Reproduced with permission. Copyright 2023 and 2024, Elsevier Publication.

2.1.3. Semiconductor Composite Modified TiO_2

Coupling TiO_2 with other semiconductors to construct heterostructures can greatly facilitate charge transfer between interfaces and promote the separation and migration of photogenerated charges, thus improving carrier utilization. Currently, the common types of heterojunctions are type-I, type-II, Z-Scheme and S-Scheme.

Cu-based semiconductor (CuO and Cu_2O), as a common visible light photocatalyst, is a good choice for TiO_2 composite due to their narrow band gap. The researchers prepared Cu_2O/(0 0 1) TiO_2 by an impregnation-reduction method and tested the removal efficiency of NH_3 under simulated sunlight. The results (Figure 3a,b) show that the removal rate of NH_3 by Cu_2O/(0 0 1)TiO_2 is 80% (The NH_3 concentration is about 120 ppm), which is higher than that of pure P25 (12%), Cu_2O (12%) and (0 0 1) TiO_2 (15%). This is due to the fact that Cu_2O promotes the exposure of the (0 0 1) TiO_2 active crystal plane and broadens the absorption range of sunlight. Further, after repeated use for 4 times, the degradation rate of NH_3 gradually decreased, which was caused by the formation of nitrates covering the reactive site [55]. Further, Zhu et al. explored the effect of the composite ratio of Cu_2O and (0 0 1) TiO_2 on the photocatalytic removal of NH_3. The results show (Figure 3c,d) that when the recombination ratio was 1:10, the specific surface area

was the largest (72.51 m^2/g) and the degradation rate of NH_3 was also maintained at 85%. However, after cycling, the catalyst was still significantly deactivated, and it was found that the surface adsorbed water and hydroxyl radical participated in the oxidation of NH_3, and finally formed nitrate species [56]. Additionally, Tihana et al. prepared Cu-modified TiO_2 nanotube arrays by wet impregnation (Figure 3e) and anodic oxidation, which have the dual roles of photocatalytic NH_3 degradation and as relative humidity sensing materials. Compared with unmodified TNT, all CuO-TNTs exhibited better NH_3 removal efficiency (Figure 3f). The CuO nanoparticles dispersed on the TiO_2 surface acted as free electron trapping sites, which reduced the rapid recombination rate of electrons and holes on the TiO_2 surface, thus promoting the photocatalytic degradation of NH_3. The above composites with Cu-based photocatalysts are anatase TiO_2, but special results are obtained when they are combined with rutile TiO_2 [57]. Chen et al. investigated the effect of charge transfer direction between CuO_x and TiO_2 (Figure 4a) on the photocatalytic degradation activity of NH_3. They observed that CuO_x/anatase TiO_2 exhibited better catalytic activity than CuO_x/rutile TiO_2 under UV irradiation. Whereas CuO_x/rutile TiO_2 had excellent photocatalytic activity under visible light irradiation, CuO_x/anatase TiO_2 was inactive. Combined with EPR and DFT calculations, they found that the crystalline phase of TiO_2 significantly affects the charge separation of CuO_x/TiO_2, leading to different charge transfer directions (Figure 4b,c). Visible light can excite electrons from the VB of rutile to CuO_x, leaving behind h^+ with high oxidation potentials that effectively oxidize NH_3, whereas at the CuO_x/anatase TiO_2 interface, visible light can only excite the electron transfer from the VB of CuO_x to the CB, and the h^+ left behind in its VB cannot oxidize NH_3 with low oxidation potentials [58].

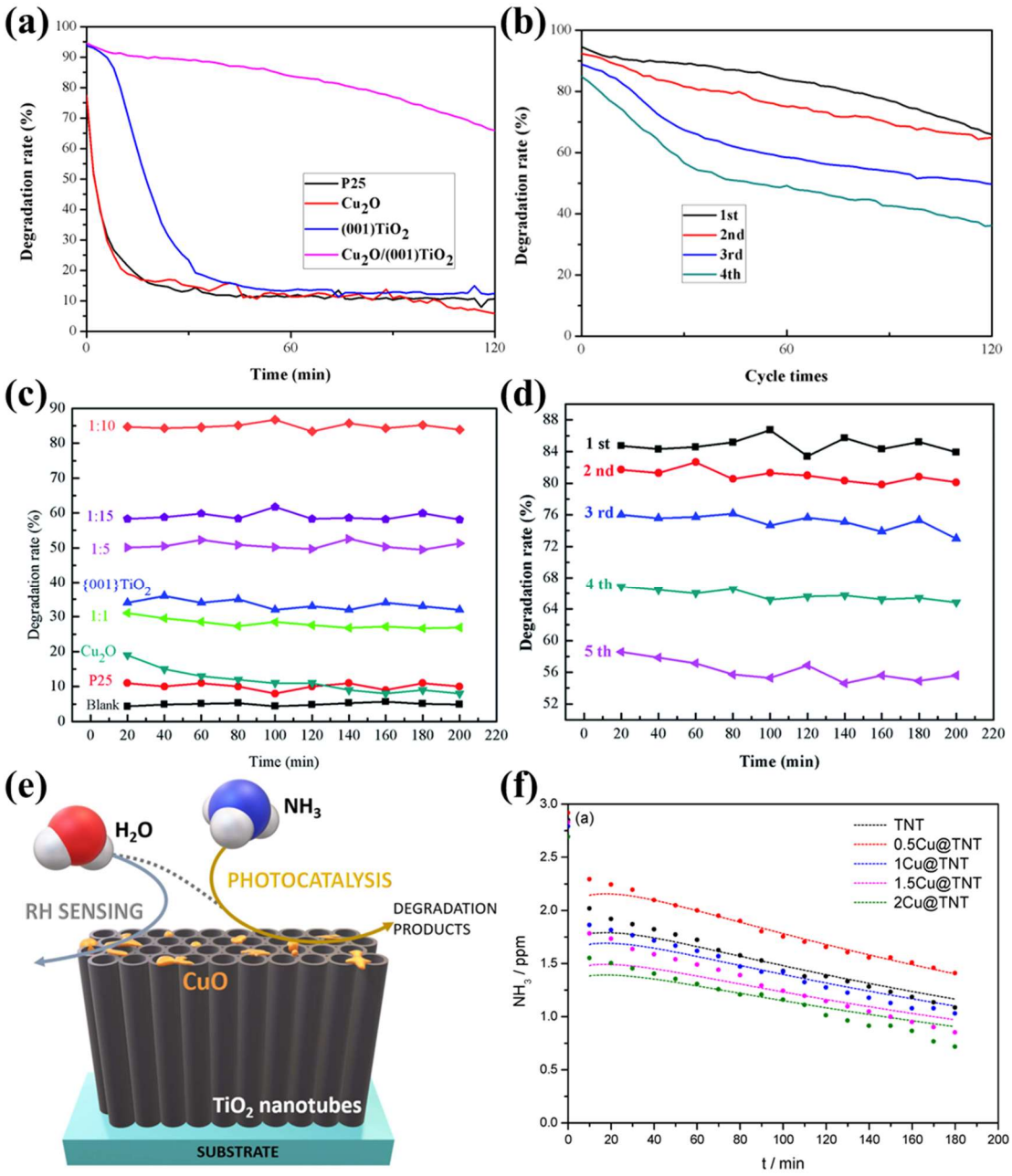

Figure 3. (**a**,**b**) The photocatalytic oxidation of NH_3 on P25, Cu_2O, (0 0 1)TiO_2 and Cu_2O/(0 0 1)TiO_2 and the NH_3 removal efficiency after cycling on Cu_2O/(0 0 1)TiO_2 under visible light [55]. Reproduced with permission. Copyright 2019, MDPI Publication. (**c**,**d**) Photocatalytic oxidation of ammonia at different Cu_2O and (0 0 1) TiO_2 composite ratios and removal efficiency of NH_3 after cycling when Cu_2O (0 0 1) is 1:10 [56]. Reproduced with permission. Copyright 2021, RSC Publication. (**e**,**f**) Photocatalytic oxidation of NH_3 on N−TiO_2, C/N−TiO_2 and pure TiO_2 under visible light [57]. Reproduced with permission. Copyright 2021, MDPI Publication.

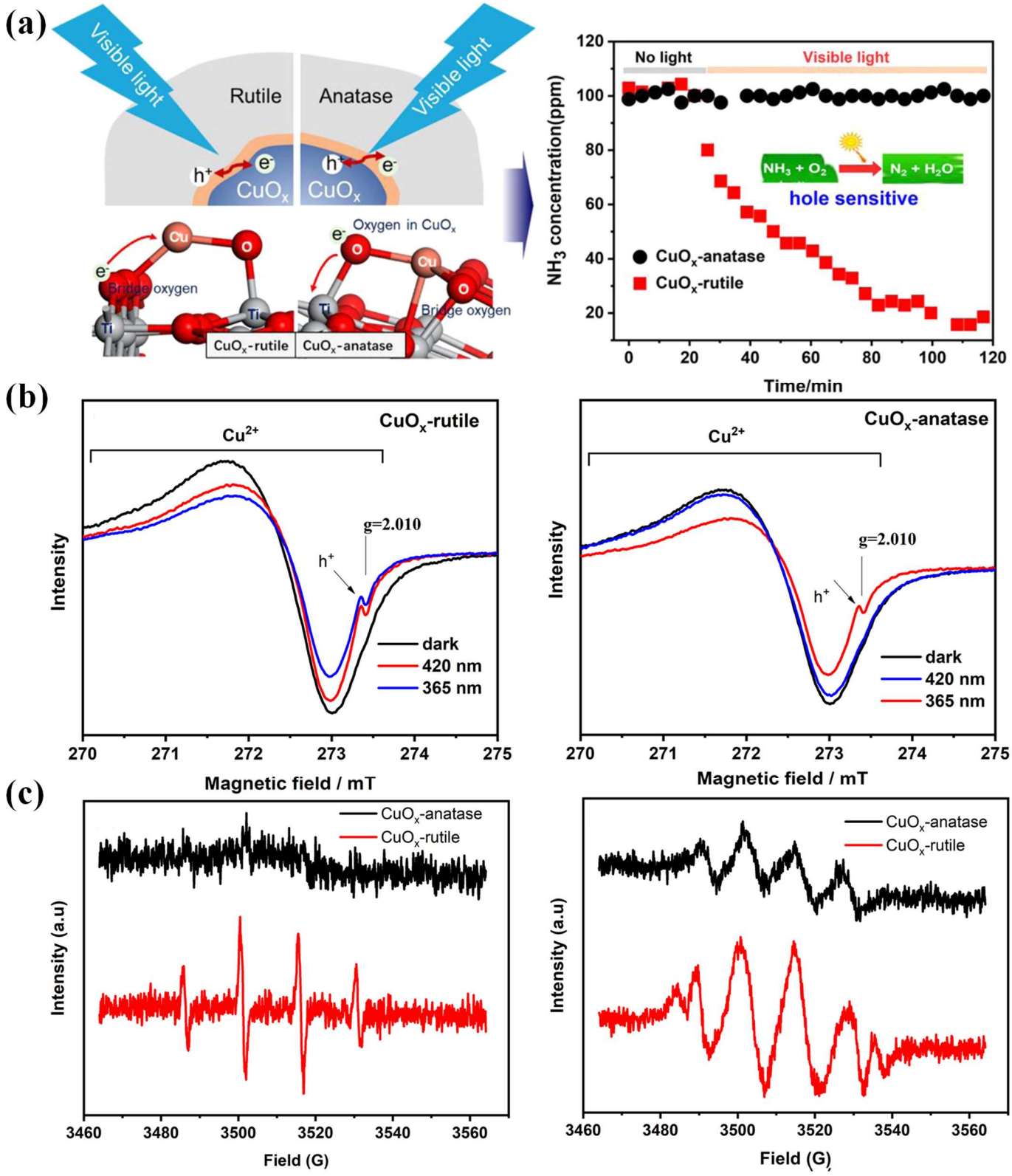

Figure 4. (**a**) Photocatalytic oxidation of NH_3 under visible light over CuO_x/anatase TiO_2 and CuO_x/rutile TiO_2. (100 ppm NH_3, 20 vol% O_2, RH = 50% and N_2 balance). (**b**) EPR spectra of CuO_x/rutile TiO_2 and CuO_x/anatase TiO_2 measured at 77 K under vacuum with visible light or UV irradiation. (**c**) DMPO spin-trapping EPR spectra measured at 303 K after 5 min visible irradiation in aqueous solutions and acetonitrile over different samples [58]. Reproduced with permission. Copyright 2022, Elsevier Publication.

In addition to Cu-based catalysts, other semiconductors have also been used to compound with TiO_2 to enhance the photocatalytic oxidation activity of NH_3. To broaden the sunlight response range, Pu et al. prepared a composite RGO/TiO_2 catalyst for NH_3 degradation in livestock farms by Hummer's method using a silica core board as a carrier. The degradation efficiency of NH_3 was as high as 93.64% under 300 W UV irradiation (Figure 5a). The introduction of RGO reduced the band gap energy of P25 from 3.14 to 2.96 eV, which enhanced the light absorption. Meanwhile, its layered pleated structure increased the adsorption of NH_3 on the surface of the material and also lowered the recombination rate of photogenerated carriers, which led to the improvement of the photocatalytic performance of P25 [59]. Further, Gao et al. prepared tetraphenyl porphyrin (TPP)-modified anatase TiO_2 by a one-step solvothermal method, which exhibited excellent photocatalytic activity under visible light irradiation, and the ammonia removal efficiency reached more than 98% within 8 h at room temperature. Under visible light irradiation, TPP contributes H to generate H^+ and VB holes with strong oxidizing ability (Figure 5b). The electrons were transferred to the TiO_2 surface via Ti−O−C bonds, which promoted the reduction of Ti^{4+} and the generation of oxygen vacancy defects. However, the accumulation of thermodynamically stable NH_4NO_3 (Figure 5c) on the catalyst surface leads to the deactivation of the photocatalyst [60].

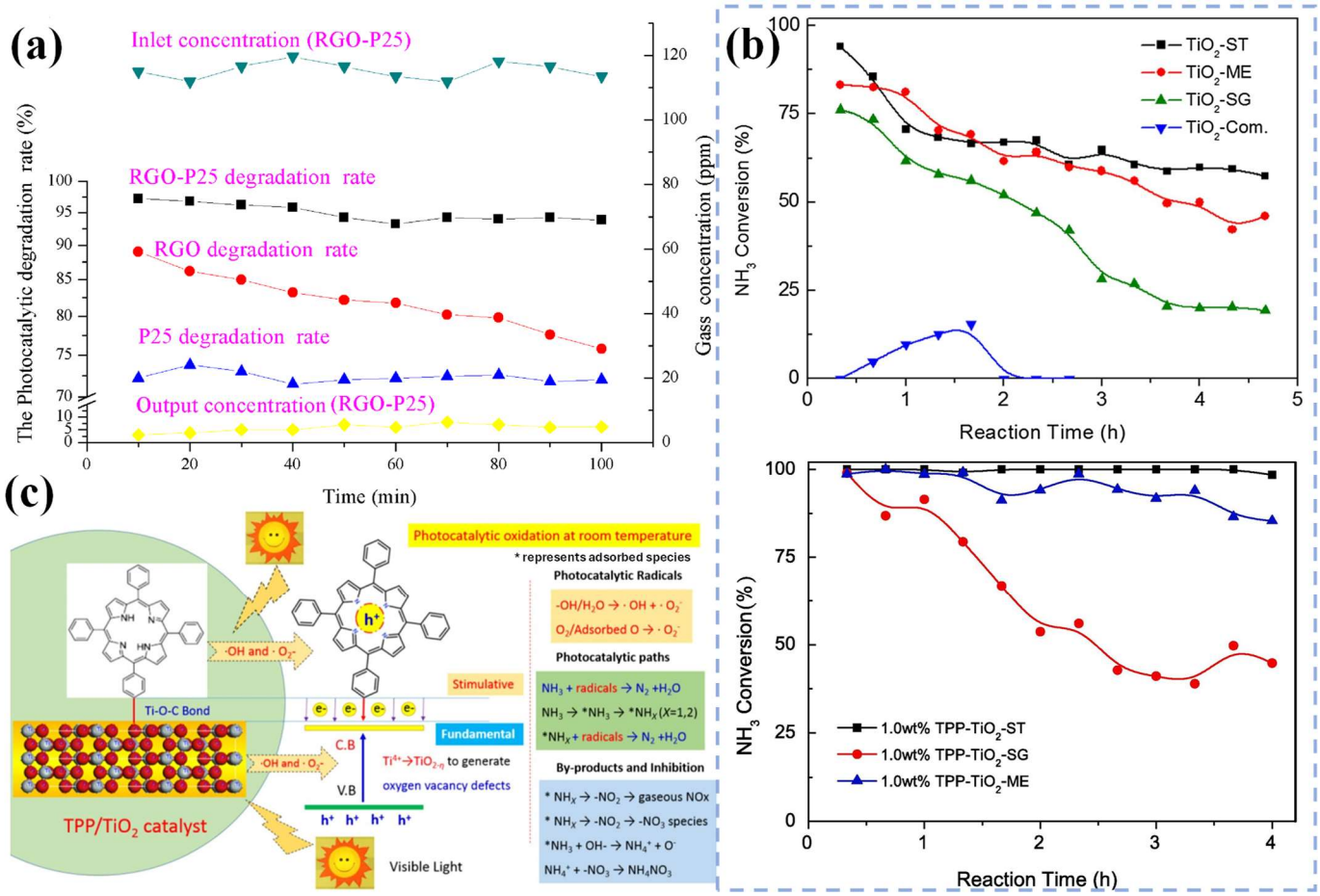

Figure 5. (**a**) The degradation effect of NH_3 by RGO-P25, RGO and P25 [59]. Reproduced with permission. Copyright 2018, MDPI Publication. (**b**) Photocatalytic activity of ammonia oxidation on different catalysts (100 ppm NH_3, 21 vol% O_2, N_2 to balance, the total flow rate of 0.2 L/min, visible light area of 47.25 cm^2, light intensity of 100 mw/cm^2). (**c**) Proposed photocatalytic oxidation mechanisms of NH_3 over TPP/TiO_2−ST catalysts under visible light irradiation [60]. Reproduced with permission. Copyright 2020, Elsevier Publication.

To enhance the capture of NH_3, the researchers also used a semiconductor coating on another photocatalyst to increase the specific surface area of the catalyst. Pu et al. prepared MoS_2@TiO_2 encapsulated carbon coaxial nanobelts (CNBs) by electrostatic spinning-hydrothermal reaction (Figure 6a) for photocatalytic degradation of NH_3. The degradation efficiency reached 91% after only 7 min of UV illumination. The introduction of carbon improved the carrier dynamics and electron affinity of TiO_2, and the larger specific surface area and layered pore structure of MoS_2@TiO_2 CNBs enhanced the adsorption of NH_3. While the construction of heterojunctions promoted the separation and migration of photogenerated charges, effectively reduced the recombination efficiency, and prolonged the lifetime

of photogenerated e^-−h^+ [61]. Similarly, Li et al. used the sol−gel method to coat TiO_2 on WO_3 nanowires (Figure 6b). After the WO_3@TiO_2 photocatalyst was exposed to simulated sunlight for 3 h, the NH_3 conversion and N_2 selectivity were found to be 58% and 94%, which were approximately double the performance of TiO_2 and WO_3 alone (Figure 6c). The enhanced photocatalytic activity is attributed to the built-in electric field between WO_3 and TiO_2, which promotes rapid charge separation and migration. In addition, the core-shell structure enhanced NH_3 adsorption and O_2 activation. This study suggests that photogenerated holes and superoxide radicals play important roles in the photocatalytic oxidation of NH_3, and efficient removal of NH_3 by constructing an interfacial electric field is an effective strategy [62]. In addition, Li et al. prepared a porous carbon framework material with a layered structure of N-doped coated ultrafine TiO_2 (N−C@TiO_2) powder by solvothermal method, which has excellent photocatalytic activity, and the removal rate of NH_3 reaches 100% after only 5 min of illumination. The N-doped porous carbon framework has a large specific surface area and good metal conductivity, which can promote the charge transfer to the interface and impede the photogenerated e^-−h^+ recombination. The increase in the concentration of h^+ on the TiO_2 surface can promote the adsorption and activation of NH_3, thus enhancing the photocatalytic activity of TiO_2 [63].

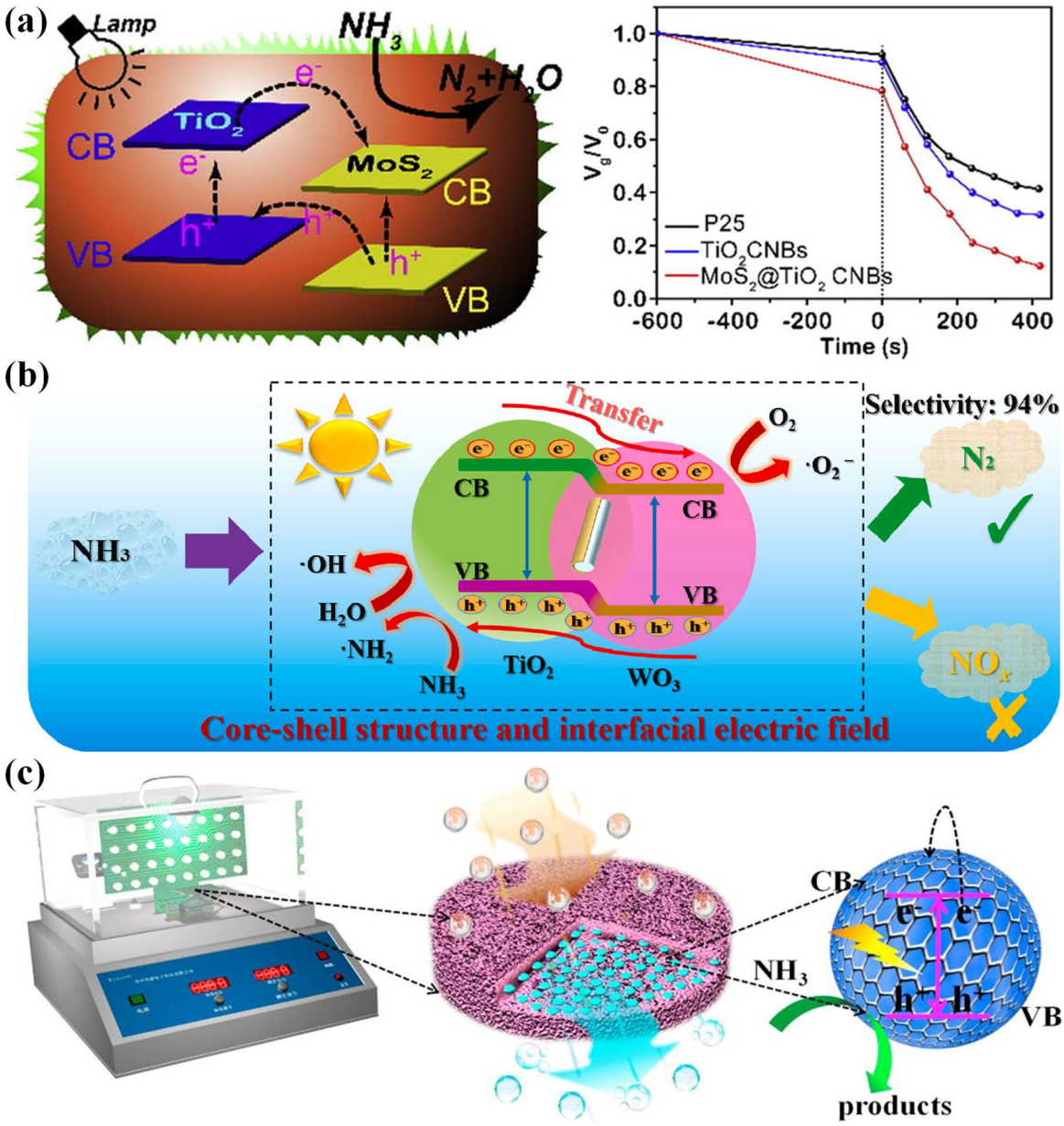

Figure 6. (**a**) Schematic illustration of the proposed photocurrent−transducer mechanism and the NH_3 degradation of P25, TiO_2 CNBs and MoS_2@TiO_2 CNBs heterojunction [61]. (**b**) Schematic illustration of the photocatalytic NH_3 oxidation mechanism over the 3WO_3@TiO_2 photocatalyst under simulated sunlight irradiation [62]. (**c**) Schematic illustration of the hierarchical structure of as−synthesized material (N−C@TiO_2) and involved electron behavior for photodegradation NH_3 [63]. Reproduced with permission. Copyright 2018, 2020 and 2024, Elsevier Publication.

For the photocatalytic oxidation of NH_3, at present, it is limited to the formation of type-II heterostructures to improve the utilization of carrier and solar energy. However, the type II heterostructure is at the expense of the Oxidation and reduction ability of the photocatalyst. Therefore, it is necessary to develop other heterogeneous structures, especially those with Z-type heterogeneous structures.

2.1.4. Metal-supported Modified TiO_2

Depositing different noble metals on the TiO_2 surface, the photogenerated electrons will continue to be transferred from TiO_2 to the metal due to the difference in their Fermi energy levels until their Fermi energy levels are similar or the same. The Schottky junction formed at the interface between the metal and TiO_2 can promote the separation of photogenerated charges. The metal acts as an electron trapping site to enrich electrons and reduce O_2 adsorbed on the surface to generate more reactive species, delaying carrier recombination.

Shu et al. investigated the effect of F or Pt modification on the catalytic activity of TiO_2 (Pt/F−TiO_2) for selective photocatalytic oxidation of NH_3. They found that surface fluorination had no significant effect on the degradation efficiency of NH_3, but it could enhance the adsorption of NH_3 on the TiO_2 surface and might reduce the generation of harmful NO_x by influencing the reaction pathway (Figure 7a). In addition, the deposited Pt prolonged the lifetime of photogenerated carriers by strongly trapping electrons, and the electron-rich Pt acted as a reduction site, providing electrons to NO_x to promote N_2 production (Figure 7b) [64].

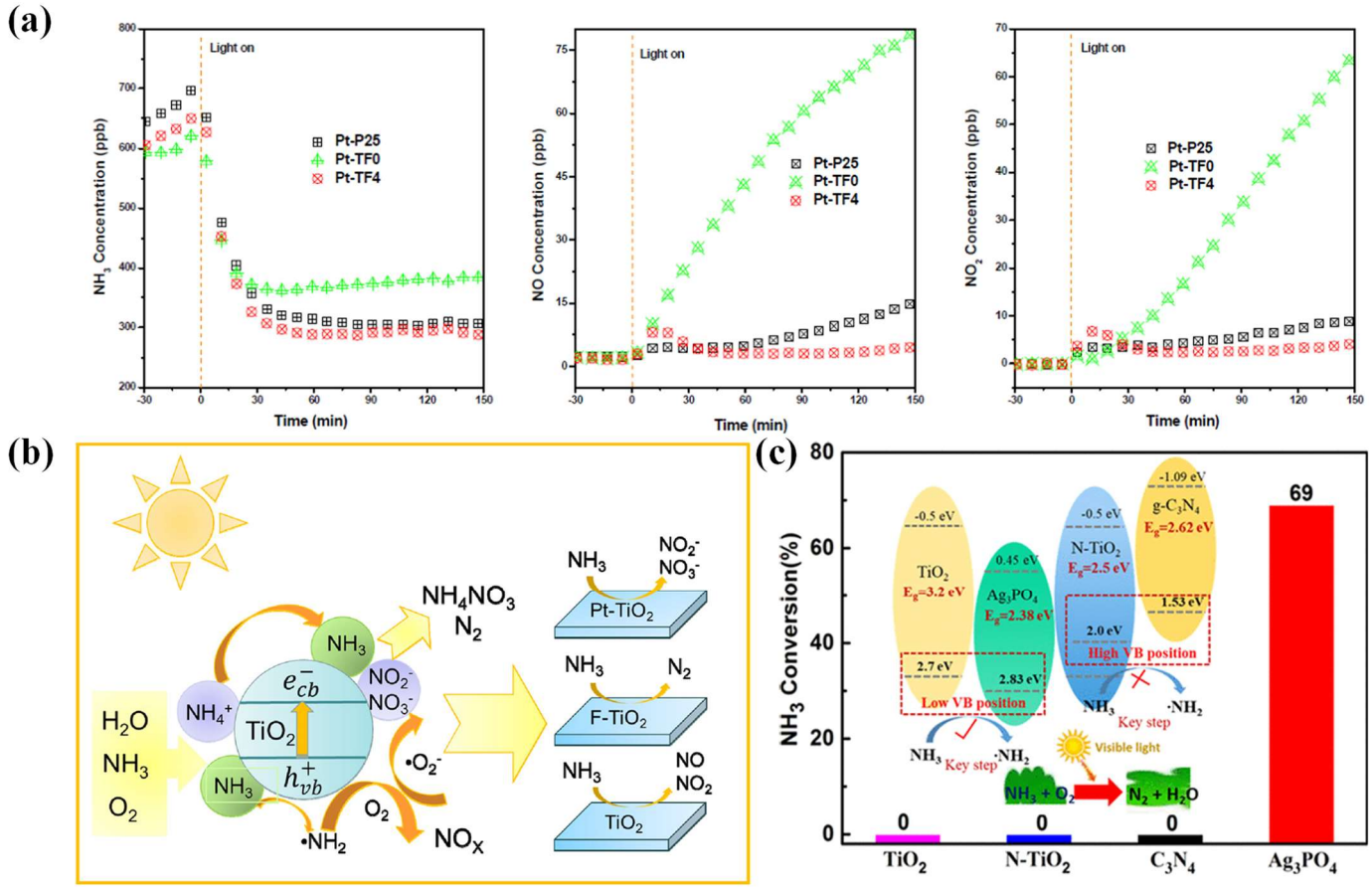

Figure 7. (**a**) Outlet NH_3 concentration, NO concentration and NO_2 concentration of different samples (Pt/P25, Pt/TF0 and Pt/TF4) under simulated sunlight irradiation. (**b**) Schematic diagram of the photocatalytic oxidation process of NH_3 on Pt/F−TiO_2 [64]. Reproduced with permission. Copyright 2022, Elsevier Publication. (**c**) Photocatalytic oxidation of NH_3 on different catalysts (TiO_2, N−TiO_2, C_3N_4 and Ag_3PO_4) under visible light [65]. Reproduced with permission. Copyright 2020, ACS Publication.

2.2. Other Photocatalysts

In addition to TiO_2 based catalysts, other photocatalysts have also been used for the photocatalytic oxidation of NH_3. He et al. prepared a series of typical visible light photocatalysts (N−TiO_2, g−C_3N_4 and Ag_3PO_4), hoping to realize the photocatalytic oxidation of NH_3 under visible light (Figure 7c). However, the results show that only Ag_3PO_4 has the removal effect in visible light. Therefore, an active, visible light photocatalyst for NH_3 oxidation requires both a suitable

band gap for visible light response and a low VB edge associated with a high oxidation potential for activating NH_3 to $\cdot NH_2$. This result also confirmed that h^+ is responsible for triggering the initial key step of NH_3 oxidation [65].

3. NH_3 Removal Mechanism

At present, researchers have deeply studied the photocatalytic oxidation mechanism of NH_3, but only limited to TiO_2 based photocatalysts. First of all, adsorption is the first step in a chemical reaction. At present, researchers generally believe that the Lewis acidic site is the active site of NH_3 photocatalytic oxidation on TiO_2 based photocatalysts [66]. NH_3 adsorbs at the Lewis acidic site will react with h^+ to form $\cdot NH_2$ for subsequent reaction under the irradiation of simulated sunlight (Equation (1)) [67,68].

$$NH_3 + h^+ \rightarrow \cdot NH_2 + H^+ \quad (1)$$

Subsequently, three oxidation pathways are divided according to the different reactive substances with $\cdot NH_2$.

(i) $\cdot NH_2$ mechanism. $\cdot NH_2$ reacts with reactive oxygen species (ROS) to form NO_x or nitrate. This mechanism has been observed on almost all NH_3 photocatalytic oxidation catalysts. The researchers explored the photocatalytic oxidation path of NH_3 on anatase TiO_2 using in-situ DRIFTS. The results showed that the $\cdot NH_2$ reacted with the oxygen anion free radical ($\cdot O_2^-$) formed under ultraviolet irradiation to form NO. Further reacting with O_2, NO was converted to NO_2^-, nitro and NO_3^- (monodentate and bidentate) substances on the TiO_2 surface (Equations (2)–(7)) [69].

$$\cdot NH_2 + O_2 \rightarrow NO + H_2O \quad (2)$$

$$NO + \cdot O_2^- \rightarrow NO_2^- \quad (3)$$

$$NO + \cdot O_2^- \rightarrow NO_3^- \quad (4)$$

$$\cdot NH_2 + \cdot O_2^- \rightarrow NO^- + H_2O \quad (5)$$

$$NO^- + O_2 \rightarrow NO_3^- \quad (6)$$

$$NO + O_2 \rightarrow NO_2 \quad (7)$$

(ii) *In-situ* selective catalytic reduction (iSCR) mechanism. By observing the reaction products of $\cdot NH_2$ mechanism, it can be found that although NH_3 is removed by photocatalytic oxidation, NO_x will be generated, which is highly likely to cause secondary pollution to the environment. In addition, the formed nitrite and nitrate will cover the active site of the photocatalyst and lead to the deactivation of the catalyst. Fortunately, NH_3 can react with the formed NO_x and nitrate to form N_2 and water, the iSCR mechanism (Equations (8)–(10)). The existence of this mechanism promotes the improvement of nitrogen selectivity. Even if NO_x is generated in the process of NH_3 photocatalytic oxidation, the final products are N_2 and water [70]. Yamazoe et al. found that $\cdot NH_2$ could selectively react with the formed monodentate and bidentate NO_3^- and NO on TiO_2 to generate N_2 under UV light irradiation. The researchers also found a similar reaction path on Pt and F co-modified TiO_2 photocatalysts. Furthermore, it is proved that h^+ and e^- play an important role in the formation of NO_x through free radical quenching experiments. When $\cdot OH$ and $\cdot O_2^-$ were removed, the production of NO_x increased significantly, indicating that $\cdot OH$ and $\cdot O_2^-$ could inhibit the formation of NO_x or rapidly oxidize NO_x to nitrate and nitrite [68]. Therefore, in the process of photocatalytic oxidation of NH_3, the above two mechanisms exist on almost all photocatalysts. That is, NH_3 is first oxidized to NO_x and nitrate by $\cdot NH_2$ mechanism and then reduced to harmless N_2 and water by the iSCR mechanism (Figure 8a,d,e).

$$NO + \cdot NH_2 \rightarrow NH_2NO \rightarrow N_2 + H_2O \quad (8)$$

$$NO_2 + \cdot NH_2 \rightarrow NH_2NO_2 \rightarrow N_2 + H_2O + O_{ads} \quad (9)$$

$$NO_3^- + NH_4^+ \rightarrow NH_4NO_3 \rightarrow N_2 + H_2O \quad (10)$$

(iii) N_2H_4 mechanism. The synergistic effect of these above two mechanisms seems to be able to treat NH_3 into harmless

N_2 and water, but due to the mismatch in the rates of the two reactions, the generated NO_x cannot be reduced to N_2 in time, and part of NO_x and nitrate will still be produced, resulting in secondary pollution. In addition, it remains to be discussed whether nitrate can be reduced to N_2 (Equation (10)), so that nitrate substances remaining on the surface will cover the active site of the reaction and lead to the deactivation of the catalyst. In this case, a new mechanism of NH_3 oxidation was discovered and proposed by the researchers. That is, $\cdot NH_2$ is coupled to form N_2H_4 species (Figure 8d), followed by dehydrogenation to form N_2H_2 species, and finally dehydrogenation to form N_2 and water (Equations (11)–(13)). The N_2H_4 pathway, which neither involves the formation of NO_x and nitrates nor leads to secondary environmental pollution and catalyst deactivation, appears to be an economically and environmentally friendly route for NH_3 removal. In the exploration of selective catalytic oxidation of NH_3, the N_2H_4 mechanism was first discovered on the Al_2O_3 catalyst supported by Pd or Ag in thermal catalytic oxidation [28,30]. Using in-situ characterization techniques, the researchers found a characteristic peak at 2170 cm^{-1} that gradually increased with the response and attributed it to the HN=NH species. Recently, the N_2H_4 mechanism has also been observed during the photocatalytic oxidation of NH_3 on Mo, C−TiO_2 photocatalyst, and it has been confirmed that the introduction of Mo ions is responsible for the existence of this mechanism [52]. Additionally, in the investigation of electrocatalytic oxidation of NH_3, the N_2H_4 mechanism has also been observed on Ru-based catalysts and the high value-added substance N_2H_4 is used as the end product (Figure 9b) [71]. In fact, the researchers also found the N_2H_4 mechanism in the reaction process of photocatalytic cracking of NH_3. The decomposition mechanism of NH_3 on Ni/TiO_2 under UV irradiation was calculated using DFT simulation (Figure 9a) [72]. The researchers simulated three NH_3 decomposition paths and calculated the activation energy of each step separately. The results showed that the maximum activation energy of route 1 is 235.7 KJ/mol, which made it almost impossible for Route 1 to react. In contrast, the highest activation energy of route 2 and route 2′ is 74.4 and 59.2 KJ/mol, respectively. Therefore, the decomposition path of NH_3 should be first coupled to generate N_2H_4 and then gradually dehydrogenation.

$$2 \cdot NH_2 \rightarrow N_2H_4 \quad (11)$$

$$N_2H_4 + 1/2O_2 \rightarrow N_2H_2 + H_2O \quad (12)$$

$$N_2H_2 + 1/2O_2 \rightarrow N_2 + H_2O \quad (13)$$

Generally, researchers have identified three mechanisms for NH_3 removal during photocatalytic oxidation: the $\cdot NH_2$ mechanism, the iSCR mechanism and the N_2H_4 mechanism. Notably, the $\cdot NH_2$ and the iSCR mechanisms often coexist in most photocatalytic oxidation processes for ammonia. In the $\cdot NH_2$ mechanism, the $\cdot NH_2$ species is oxidized to NO, NO_2 or nitrate. Subsequently, the generated NO_x reacts with $\cdot NH_2$ molecules via the iSCR mechanism, resulting in the production of harmless N_2 and water, thereby ensuring N_2 selectivity in the photocatalytic process. However, the mismatch between the reaction rates of these two mechanisms can easily lead to the release of NO_x and the deactivation of the catalyst due to nitrate accumulation on the catalyst surface. In response to this challenge, the N_2H_4 mechanism has emerged as a promising alternative for ammonia removal. The N_2H_4 species can gradually dehydrogenate to produce N_2 and water without generating NO_x or nitrate, thereby preventing secondary environmental pollution and reducing catalyst deactivation.

In addition, humidity also has an important effect on the NH_3 oxidation mechanism under environmental conditions. The researchers explored the path of photocatalytic oxidation of ppb level NH_3 on TiO_2 and explored the role of water in the process. Below 50% relative humidity, water catalyzed reactions that promote NO_x formation. However, above 50%, the increase in adsorbed water hindered the contact of active sites, promoted the formation of non-reactive NH_4^+, and reduced oxidant levels, thereby decreasing NO_x formation [73]. The researchers used a coated wall flow tube and a chemiluminescence NO_x analyzer to study the kinetics of NH_3 absorption and NO_x formation on irradiated TiO_2 surfaces. They found that NH_3 absorption kinetics are inversely proportional to NH_3 concentration, indicating adherence to the Langmuir-Hinshelwood mechanism. The first step of the reaction involved a collision reaction between NH_3 and valence band holes on the TiO_2 surface, generating $\cdot NH_2$. $\cdot NH_2$ reacted with O_2 to form amino peroxy radicals (NH_2OO), a reaction that proceeded more rapidly in the aqueous phase. NH_2OO undergoes water-catalyzed isomerization and decomposition reactions to produce NO, which was further oxidized to NO_2 on the TiO_2 surface. Water plays a crucial catalytic role throughout the reaction mechanism (Figure 8c). Theoretical calculations supported the experimental results, indicating that the solvation of key intermediates facilitates proton transfer isomerization, making the NO formation step exothermic. The NO_x produced by the P25 photocatalyst was twice that of anatase, while the reactivity

of rutile was less than 10% of anatase. This is due to differences in their E_g, adsorption capacity, and electron-hole recombination efficiency.

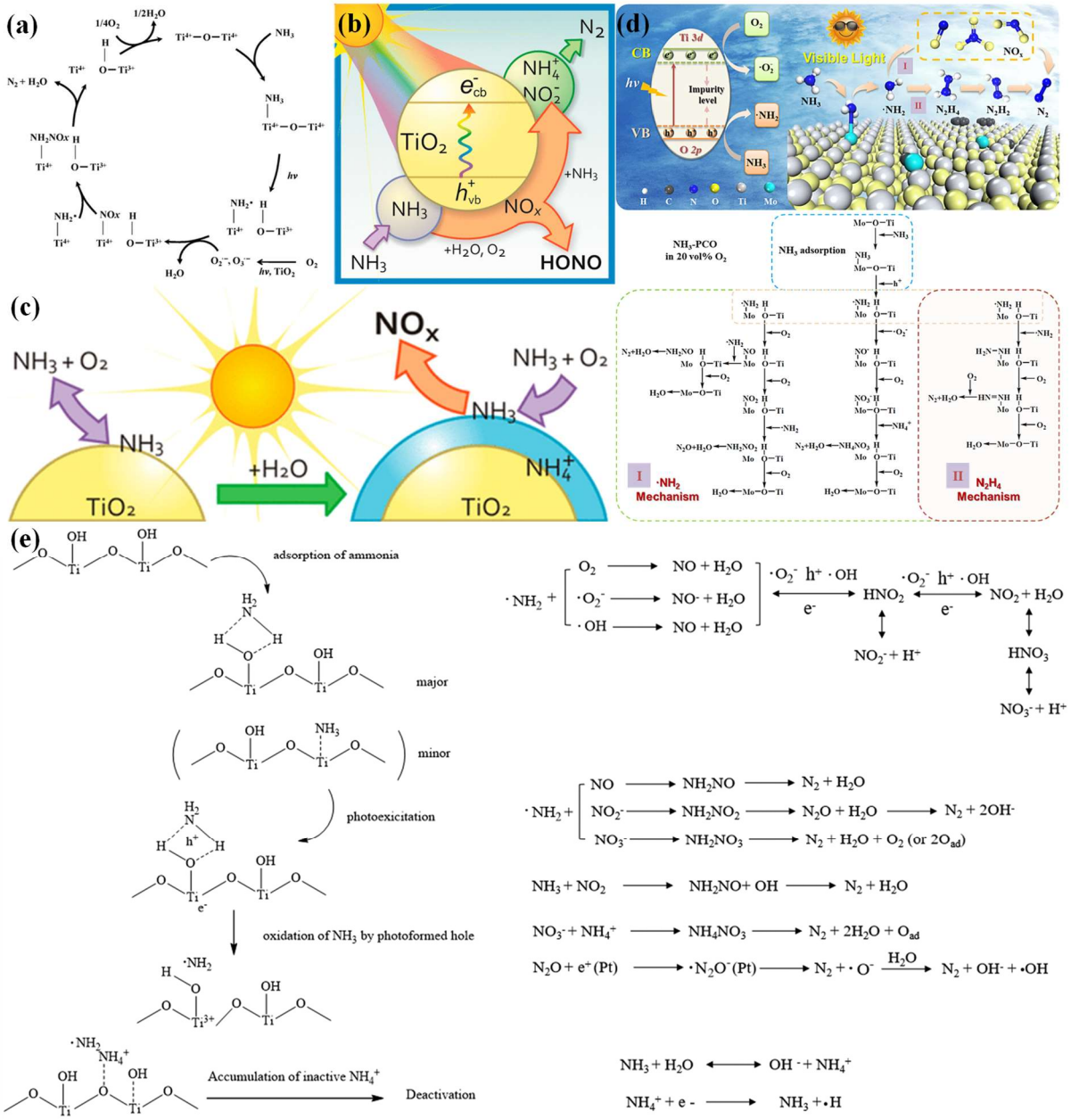

Figure 8. (**a**) Mechanism of photocatalytic oxidation of NH_3 on TiO_2 [69]. Reproduced with permission. Copyright 2008, Elsevier Publication. (**b**) NH_3 photooxidation in air forms HONO on TiO_2 when RH = 48% [74]. Reproduced with permission. (**c**) NH_3 will be photo-oxidized to NO_x on TiO_2 under the catalysis of water [73]. Copyright 2013, ACS Publication. (**d**) The proposed N_2H_4 mechanism of NH_3 photo-oxidation on Mo, C−TiO_2 [52]. (**e**) Mechanism of photocatalytic oxidation of NH_3 on Pt/F−TiO_2 (·NH_2 and iSCR mechanism) [64]. Reproduced with permission. Copyright 2022 and 2024, Elsevier Publication.

In other work, Kebede et al. indicated that (Figure 8b) TiO_2 could convert NH_3 into HONO under light exposure, which resulted from the reduction of NO_2 and NO_3^- produced by the photooxidation of NH_3 catalyzed by water. HONO is a form of NO_x in the atmosphere that can generate ozone and other secondary pollutants through photochemical reactions, thereby exacerbating air pollution [74]. Exposure to high concentrations of HONO may have adverse effects on human health. It can irritate the respiratory tract and trigger or worsen asthma and other respiratory diseases. The results showed that the amount of HONO formed depends on the initial NH_3 concentration and the relative humidity of the carrier gas. The highest HONO yield, reaching 350 ppb, was observed at moderate NH_3 concentrations (150–290 ppb) and 30–40% relative humidity. However, when the relative humidity increased from 40% to 95%, the HONO yield decreased from 350 ppt to 50 ppt. This was consistent with previous studies on the photocatalytic oxidation of NH_3 to nitrogen dioxide by TiO_2, suggesting that at relative humidity below 40%, water-promoted reactions favor the formation

of nitrogen dioxide. In contrast, at relative humidity above 40%, capillary condensation filled the micropores on the TiO_2 surface, hindering access to reactive sites and thus reducing the formation of NO_2 and HONO. When NH_3 concentration exceeded 290 ppb, the formation of HONO decreased, possibly due to the reaction (iSCR mechanism) between HONO and NH_3.

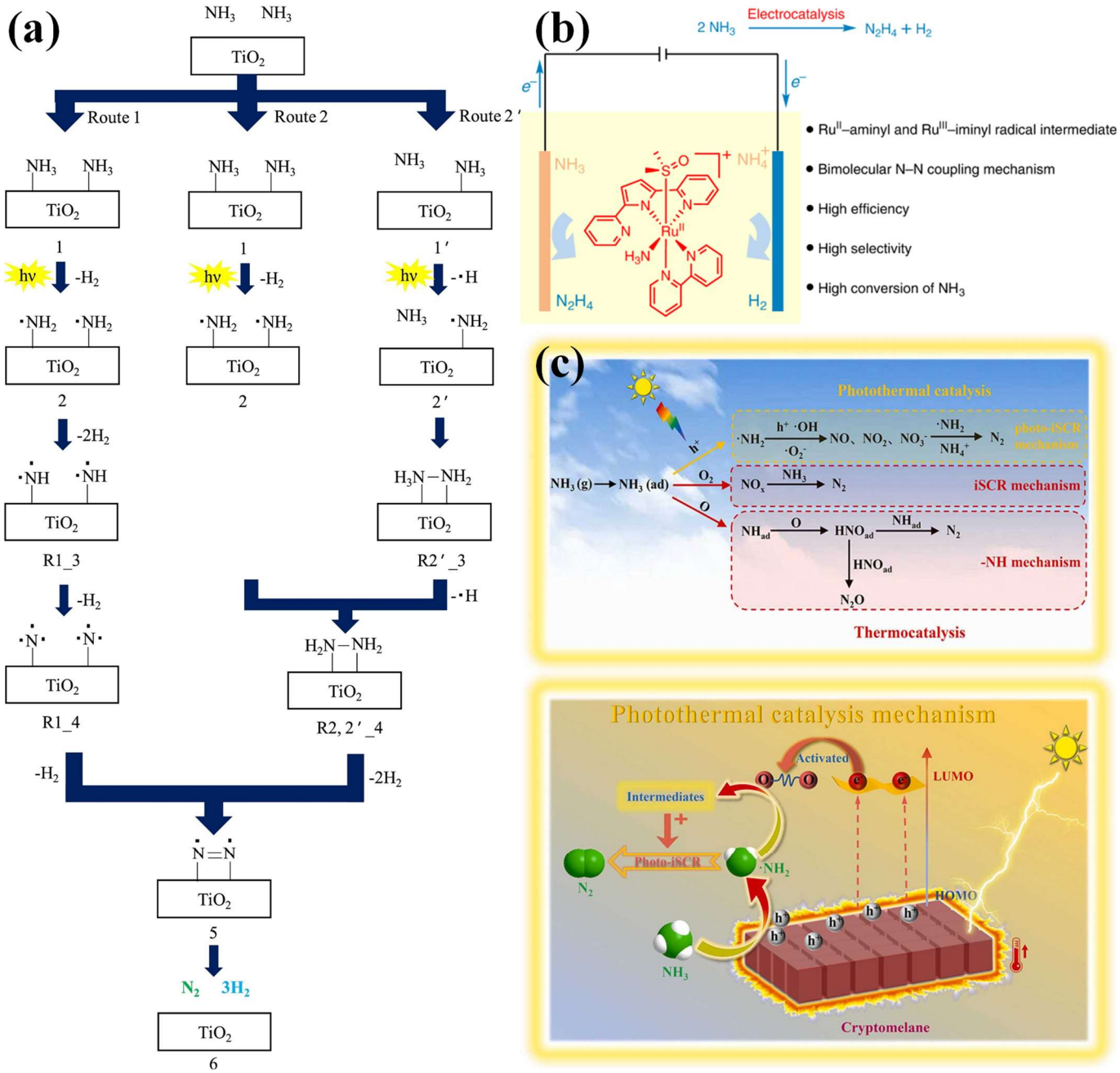

Figure 9. (**a**) Reaction mechanism for NH_3 decomposition to N_2 and H_2 over TiO_2 photocatalyst [72]. Reproduced with permission. Copyright 2017, Elsevier Publication. (**b**) Mechanism of electrocatalytic oxidation of NH_3 to N_2H_4 [71]. Reproduced with permission. Copyright 2023, Springer Nature Publication. (**c**) Mechanism of photothermal synergistic catalytic oxidation of NH_3 and oxidation path of NH_3 [75]. Reproduced with permission. Copyright 2023, Elsevier Publication.

Therefore, optimal relative humidity (RH) levels can enhance the removal efficiency of photocatalyzed NH_3 oxidation. However, excessive RH can hinder the adsorption of NH_3 molecules due to the presence of water, which simultaneously catalyzes the formation of NO_x. This interaction can lead to a reduction in both the reaction activity of the catalyst and its selectivity for N_2.

4. Challenges and Prospects of Photocatalytic Oxidation of NH_3

Photocatalytic oxidation as a promising NH_3 treatment strategy is being gradually improved, but there are still many challenges. However, the catalysts for the photocatalytic oxidation of NH_3 have been studied in depth, including the performance and oxidation mechanism. However, it is only limited to TiO_2 based catalysts, and other kinds of photocatalysts are rarely studied. In addition, due to the narrow range of photo-response and low utilization of charge carriers, the removal efficiency of photocatalytic oxidation does not meet the requirements of practical applications. Furthermore, NO_x or nitrate produced by the $\cdot NH_2$ mechanism cannot be reduced to N_2 and water in time, resulting in insufficient nitrogen selectivity of the reaction products. As a result, the accumulated NO_x may cause secondary pollution to the air, and the nitrate remaining on the surface of the photocatalyst will lead to the deactivation of the catalyst, increasing the cost of treatment. To solve the above problems, researchers use the heat generated by light irradiation to improve the utilization rate of solar energy and charge carriers through photothermal synergistic catalysis. For a flow with an NH_3 concentration of about 45 ppm, the NH_3 conversion rate of 91.7% and N_2 selectivity of 94.7% were obtained on the Cryptomelane nanowires (Figure 9c) [75]. Since photothermal co-catalysis had higher solar energy and carrier utilization than photocatalysis alone, it seems to be more suitable for ammonia treatment. However, it could be seen from the experimental results of cyclic on-off light that the photocatalyst still had an obvious deactivation phenomenon. This was because the experimental results confirmed that the oxidation mechanism of NH_3 was the coexistence of $\cdot NH_2$ and iSCR mechanism, indicating that there was still the formation of NO_x and nitrate, which may still cause secondary environmental pollution and catalyst deactivation. Therefore, the development of photocatalysts with N_2H_4 mechanism as the main oxidation path seems to be the key to solving this problem. Because NH_3 oxidation removal through this mechanism will not produce NO_x resulting in secondary pollution of the environment, nor will nitrate occupy the reactive active site.

In summary, with the gradual increase in human demand for NH_3, the environmental pollution caused by NH_3 is becoming increasingly serious. Due to the characteristics of discrete emission and low concentration, the traditional methods of treating gaseous pollutants are difficult to remove and high cost. In contrast, photocatalytic oxidation is an economical and practical strategy. However, the existing photocatalyst solar energy and carrier utilization rate are not high enough, resulting in the removal effect of NH_3 is not ideal. Currently, traditional methods such as metal loading, semiconductor compounding, and surface modification are employed to enhance ammonia removal efficiency and N_2 selectivity. Additionally, further research is needed to explore the application of other emerging photocatalyst modification strategies in the photocatalytic oxidation of NH_3, including semiconductor quantum dots, alloy loading, and metal phosphides [76,77]. In addition, the $\cdot NH_2$ mechanism will produce NO_x and nitrate. Although the iSCR mechanism will reduce part of NO_x to produce N_2 and water, it may still cause secondary environmental pollution and catalyst deactivation. Therefore, the exploration of photocatalysts with high removal performance and N_2H_4 mechanism as the NH_3 oxidation path may be a promising strategy to solve the NH_3 pollution problem in the future.

Acknowledgments

The authors express gratitude to the National Key Technology Research and Development Project of China (2019YFC1906404) for providing financial support for this study.

Author Contributions

Y.W.: Writing—original draft, Investigation, Formal analysis. Y.Y.: Writing—review & editing. Y.G.: Writing—review & editing, Investigation. S.Y.: Writing—review & editing, Supervision, Resources, Project administration, Funding acquisition, Conceptualization.

Ethics Statement

Not applicable.

Informed Consent Statement

Not applicable.

Funding

This research was funded by the National Key Technology Research and Development Project of China (2019YFC1906404).

Declaration of Competing Interest

The authors declare that they have no known competing financial interests or personal relationships that could have appeared to influence the work reported in this paper.

References

1. Shu Y, Wang D, Wang J, Huang H. Adsorption and photocatalytic degradation of Ammonia: Status and challenges. *Chem. Eng. J.* **2024**, *498*, 154925.
2. Afif A, Radenahmad N, Cheok Q, Shams S, Kim JH, Azad AK. Ammonia−fed fuel cells: a comprehensive review. *Renew. Sustain. Energy Rev.* **2016**, *60*, 822–835.
3. Berwal P, Kumar S, Khandelwal B. A comprehensive review on synthesis, chemical kinetics, and practical application of ammonia as future fuel for combustion. *J. Energy Inst.* **2021**, *99*, 273–298.
4. Jeerh G, Zhang M, Tao S. Recent progress in ammonia fuel cells and their potential applications. *J. Mater. Chem. A* **2021**, *9*, 727–752.
5. Jiang J, Gao F, Wang S, Tang X, Lu M, Wang J, et al. Advances in photo-catalytic oxidation of NH_3 over modified TiO_2 catalysts: Reaction pathways, improvement strategy and promotion mechanism. *J. Environ. Chem. Eng.* **2023**, *11*, 110602.
6. Vikrant K, Kim K−H, Dong F, Giannakoudakis DA. Photocatalytic Platforms for Removal of Ammonia from Gaseous and Aqueous Matrixes: Status and Challenges. *ACS Catal.* **2020**, *10*, 8683–8716.
7. Xu P, Li G, Zheng Y, Fung JCH, Chen A, Zeng Z, et al. Fertilizer management for global ammonia emission reduction. *Nature* **2024**, *626*, 792–798.
8. Chang Y, Zou Z, Zhang Y, Deng C, Hu J, Shi Z, et al. Assessing Contributions of Agricultural and Nonagricultural Emissions to Atmospheric Ammonia in a Chinese Megacity. *Environ. Sci. Technol.* **2019**, *53*, 1822–1833.
9. Nie E, Zheng G, Shao Z, Yang J, Chen T. Emission characteristics and health risk assessment of volatile organic compounds produced during municipal solid waste composting. *Waste Manag.* **2018**, *79*, 188–195.
10. Vikrant K, Roy K, Kim K−H, Bhattacharya SS. Insights into the storage stability of ammonia in polyester aluminum bags. *Environ. Res.* **2019**, *177*, 108596.
11. Schwartz−Narbonne H, Jones SH, Donaldson DJ. Indoor Lighting Releases Gas Phase Nitrogen Oxides from Indoor Painted Surfaces. *Environ. Sci. Technol. Lett.* **2019**, *6*, 92–97.
12. Photiou P, Kallis M, Samanides CG, Vyrides I, Padoan E, Montoneri E, et al. Integrated Chemical Biochemical Technology to Reduce Ammonia Emission from Fermented Municipal Biowaste. *Environ. Sci. Technol. Lett.* **2021**, *9*, 8402–8413.
13. Liu T, Wang X, Wang B, Ding X, Deng W, Lü S, et al. Emission factor of ammonia (NH_3) from on−road vehicles in China: Tunnel tests in urban Guangzhou. *Environ. Res. Lett.* **2014**, *9*, 064027.
14. Huang C, Hu Q, Lou S, Tian J, Wang R, Xu C, et al. Ammonia Emission Measurements for Light−Duty Gasoline Vehicles in China and Implications for Emission Modeling. *Environ. Res. Lett.* **2018**, *52*, 11223–11231.
15. Hopke PK, Querol X. Is Improved Vehicular NOx Control Leading to Increased Urban NH_3 Emissions? *Environ. Res. Lett.* **2022**, *56*, 11926–11927.
16. Farren NJ, Davison J, Rose RA, Wagner RL, Carslaw DC. Underestimated Ammonia Emissions from Road Vehicles. *Environ. Res. Lett.* **2020**, *54*, 15689–15697.
17. Chen Z−L, Song W, Hu C−C, Liu X−J, Chen G−Y, Walters WW, et al. Significant contributions of combustion−related sources to ammonia emissions. *Nat. Commun.* **2022**, *13*, 7710.
18. Xu W, Zhao Y, Wen Z, Chang Y, Pan Y, Sun Y, et al. Increasing importance of ammonia emission abatement in PM2.5 pollution control. *Sci. Bull.* **2022**, *67*, 1745–1749.
19. Liu Y, Zhan J, Zheng F, Song B, Zhang Y, Ma W, et al. Dust emission reduction enhanced gas−to−particle conversion of ammonia in the North China Plain. *Nat. Commun.* **2022**, *13*, 6887.
20. Gu B, Zhang L, Van Dingenen R, Vieno M, Van Grinsven HJ, Zhang X, et al. Abating ammonia is more cost−effective than nitrogen oxides for mitigating $PM_{2.5}$ air pollution. *Science* **2021**, *374*, 758–762.
21. Liu Z, Rieder HE, Schmidt C, Mayer M, Guo Y, Winiwarter W, et al. Optimal reactive nitrogen control pathways identified for cost−effective PM2.5 mitigation in Europe. *Nat. Commun.* **2023**, *14*, 4246.
22. Zhou S, Li Y, Liao X, Wang W, Mao C, Mi J, et al. A low−cost deodorizing spray net device for the removal of ammonia emissions in livestock houses. *J. Clean. Prod.* **2021**, *318*, 128516.

23. Hu T−T, Liu F, Dou S, Zhong L−B, Cheng X, Shao Z−D, et al. Selective adsorption of trace gaseous ammonia from air by a sulfonic acid−modified silica xerogel: Preparation, characterization and performance. *Chem. Eng. J.* **2022**, *443*, 136357.
24. Gebreegziabher TB, Wang S, Nam H. Adsorption of H_2S, NH_3 and TMA from indoor air using porous corncob activated carbon: Isotherm and kinetics study. *J. Environ. Chem. Eng.* **2019**, *7*, 103234.
25. Han X, Lu W, Chen Y, da Silva I, Li J, Lin L, et al. High Ammonia Adsorption in MFM−300 Materials: Dynamics and Charge Transfer in Host–Guest Binding. *J. Am. Chem. Soc.* **2021**, *143*, 3153–3161.
26. Ma B, LaPara TM, Kim T, Hozalski RM. Multi−scale Investigation of Ammonia−Oxidizing Microorganisms in Biofilters Used for Drinking Water Treatment. *J. Am. Chem. Soc.* **2023**, *57*, 3833–3842.
27. Liu J, Li X, Xu Y, Wu Y, Wang R, Zhang X, et al. Highly efficient reduction of ammonia emissions from livestock waste by the synergy of novel manure acidification and inhibition of ureolytic bacteria. *Environ. Int.* **2023**, *172*, 107768.
28. Wang F, Ma J, He G, Chen M, Zhang C, He H. Nanosize Effect of Al_2O_3 in Ag/Al_2O_3 Catalyst for the Selective Catalytic Oxidation of Ammonia. *ACS Catal.* **2018**, *8*, 2670–2682.
29. Wang F, He G, Zhang B, Chen M, Chen X, Zhang C, et al. Insights into the Activation Effect of H_2 Pretreatment on Ag/Al_2O_3 Catalyst for the Selective Oxidation of Ammonia. *ACS Catal.* **2019**, *9*, 1437–1445.
30. Dann EK, Gibson EK, Blackmore RH, Catlow CRA, Collier P, Chutia A, et al. Structural selectivity of supported Pd nanoparticles for catalytic NH_3 oxidation resolved using combined operando spectroscopy. *Nat. Catal.* **2019**, *2*, 157–163.
31. Kobayashi H, Hayakawa A, Somarathne KDKA, Okafor EC. Science and technology of ammonia combustion. *Proc. Combust. Inst.* **2019**, *37*, 109–133.
32. Kuk SK, Ji SM, Kang S, Yang DS, Kwon HJ, Koo MS, et al. Singlet−oxygen−driven photocatalytic degradation of gaseous formaldehyde and its mechanistic study. *Appl. Catal. B* **2023**, *328*, 122463.
33. Fan H, Wang R. Low−temperature NH_3−SCR reaction over 3D Cu/Fe−TiO_2−rGO composite catalyst synthesized by photoreduction method. *Appl. Catal. B* **2022**, *450*, 138152.
34. Guo Q, Zhou C, Ma Z, Ren Z, Fan H, Yang X. Elementary photocatalytic chemistry on TiO_2 surfaces. *Chem. Soc. Rev.* **2016**, *45*, 3701–3730.
35. Akhter P, Nawaz S, Shafiq I, Nazir A, Shafique S, Jamil F, et al. Efficient visible light assisted photocatalysis using ZnO/TiO_2 nanocomposites. *Mol. Catal.* **2023**, *535*, 112896.
36. Guo L, Zhang J, Zhang X, Wang R, Jia Y, Long H. Energy band matching Bi_2WO_6/black−TiO_2 Z−scheme heterostructure for the enhanced visible−light photocatalytic degradation of toluene. *Mol. Catal.* **2023**, *550*, 113603.
37. Shang F−K, Li Y−H, Qi M−Y, Tang Z−R, Xu Y−J. Photocatalytic materials for sustainable chemistry via cooperative photoredox catalysis. *Catal. Today* **2023**, *410*, 85–101.
38. Zhang Y, Qi M−Y, Tang Z−R, Xu Y−J. Photoredox−Catalyzed Plastic Waste Conversion: Nonselective Degradation versus Selective Synthesis. *ACS Catal.* **2023**, *13*, 3575–3590.
39. Huang L, He G, Yuan Y, Zhang TC, Wang Y, Yuan S. Trivalent Metal Ions (Al, Ga, In)−Doped TiO_2 for Enhanced Photocatalytic Desulfurization of H_2S: Band Structure Regulation, Performance, and Mechanism. *Ind. Eng. Chem. Res.* **2024**, *63*, 7154–7165.
40. Huang L, Yuan Y, Wang Y, Yılmaz M, Zhang TC, Yuan S. Visible−Light−Driven photocatalytic oxidation of H_2S by Boron−doped TiO_2/LDH Heterojunction: Synthesis, performance, and reaction mechanism. *Chem. Eng. J.* **2022**, *448*, 137607.
41. Guo Q, Zhou C, Ma Z, Yang X. Fundamentals of TiO_2 Photocatalysis: Concepts, Mechanisms, and Challenges. *Adv. Mater.* **2019**, *31*, 1901997.
42. Wu H, Ma J, Zhang C, He H. Effect of TiO_2 calcination temperature on the photocatalytic oxidation of gaseous NH_3. *J. Environ. Sci.* **2014**, *26*, 673–682.
43. Heylen S, Smet S, Laurier KGM, Hofkens J, Roeffaers MBJ, Martens JA. Selective photocatalytic oxidation of gaseous ammonia to dinitrogen in a continuous flow reactor. *Catal. Sci. Technol.* **2012**, *2*, 1802.
44. Sola AC, Sousa DG, Araña J, Díaz OG, Rodríguez JMD, de la Piscina PR, et al. Differences in the vapour phase photocatalytic degradation of ammonia and ethanol in the presence of water as a function of TiO_2 characteristics and the presence of O_2. *Catal. Today* **2016**, *266*, 53–61.
45. Wu H, Ma J, Li Y, Zhang C, He H. Photocatalytic oxidation of gaseous ammonia over fluorinated TiO_2 with exposed (001) facets. *Appl. Catal. B* **2014**, *152–153*, 82–87.
46. Chen M, Ma J, Zhang B, He G, Li Y, Zhang C, et al. Remarkable synergistic effect between {001} facets and surface F ions promoting hole migration on anatase TiO_2. *Appl. Catal. B* **2017**, *207*, 397–403.
47. Chen M, Ma J, Zhang B, Wang F, Li Y, Zhang C, et al. Facet−dependent performance of anatase TiO_2 for photocatalytic oxidation of gaseous ammonia. *Appl. Catal. B* **2018**, *223*, 209–215.
48. Saoud WA, Assadi AA, Guiza M, Bouzaza A, Aboussaoud W, Soutrel I, et al. Abatement of ammonia and butyraldehyde under non−thermal plasma and photocatalysis: Oxidation processes for the removal of mixture pollutants at pilot scale. *Chem. Eng. J.* **2018**, *344*, 165–172.
49. Wang P, Shen Z, Xia Y, Wang H, Zheng L, Xi W, et al. Atomic Insights for Optimum and Excess Doping in Photocatalysis: A Case Study of Few−Layer Cu−$ZnIn_2S_4$. *Adv. Funct. Mater.* **2019**, *29*, 1807013.

50. Wang S, Yu H, Cheng X. Degradation of Typical Indoor Air Pollutants Using Fe−Doped TiO_2 Thin Film under Daylight Illumination. *J. Chem.* **2014**, *2014*, 1–5.
51. Sirivallop A, Areerob T, Chiarakorn S. Enhanced Visible Light Photocatalytic Activity of N and Ag Doped and Co−Doped TiO_2 Synthesized by Using an In−Situ Solvothermal Method for Gas Phase Ammonia Removal. *Catalysts* **2020**, *10*, 251.
52. Wang Y, Huang L, Zhang TC, Wang Y, Yuan S. Visible−Light−Induced photocatalytic oxidation of gaseous ammonia on Mo, c−codoped TiO_2: Synthesis, performance and mechanism. *Chem. Eng. J.* **2024**, *482*, 148811.
53. Jiang J, Gao F, Zhang J, Lu M, Sun L, Lei Y, et al. Enhancing activity and non−deactivating stability on N−modified TiO_2 catalyst for visible−light photocatalytic oxidation of ammonia at room temperature. *Appl. Surf. Sci.* **2024**, *651*, 159238.
54. Gao F, Zhang J, Jiang J, Tang X, Zhou Y, Yi H. Visible light−induced photocatalytic oxidation of gaseous ammonia on C surface−coated N−TiO_2 catalyst: Synthesis, properties and mechanism. *Appl. Surf. Sci.* **2025**, *358*, 130349.
55. Pu S, Wang H, Zhu J, Li L, Long D, Jian Y, et al. Heterostructure Cu_2O/(001)TiO_2 Effected on Photocatalytic Degradation of Ammonia of Livestock Houses. *Catalysts* **2019**, *9*, 267.
56. Zhu J, Jian Y, Long D, Wang H, Zeng Y, Li J, et al. Degradation of ammonia gas by Cu_2O/{001}TiO_2 and its mechanistic analysis. *RSC Adv.* **2021**, *11*, 3695–3702.
57. Čižmar T, Grčić I, Bohač M, Razum M, Pavić L, Gajović A. Dual Use of Copper−Modified TiO_2 Nanotube Arrays as Material for Photocatalytic NH_3 Degradation and Relative Humidity Sensing. *Coatings* **2021**, *11*, 1500.
58. Chen M, Chen J, Chen C, Zhang C, He H. Distinct photocatalytic charges separation pathway on CuO_x modified rutile and anatase TiO_2 under visible light. *Appl. Catal. B* **2022**, *300*, 120735.
59. Pu S, Long D, Liu Z, Yang F, Zhu J. Preparation of RGO−P25 Nanocomposites for the Photocatalytic Degradation of Ammonia in Livestock Farms. *Catalysts* **2018**, *8*, 189.
60. Gao F, Song S, Tang X, Yi H, Zhao S, Yu Q. Tetraphenyl–porphyrin decorated anatase TiO_2 catalysts for the visible–light photocatalytic oxidation of gaseous ammonia at room temperature. *Appl. Surf. Sci.* **2020**, *506*, 144421.
61. Zhang H, Gu Q−Q, Zhou Y−W, Liu S−Q, Liu W−X, Luo L, et al. Direct Z−scheme photocatalytic removal of ammonia via the narrow band gap MoS_2/N−doped graphene hybrid catalyst upon near−infrared irradiation. *Appl. Surf. Sci.***2020**, *504*, 144065.
62. Li Z, Li D, Feng Z, Lv S, Zhang Q, Yu Y, et al. Enhanced photocatalytic ammonia oxidation over WO_3@TiO_2 heterostructures by constructing an interfacial electric field. *Chemosphere* **2024**, *355*, 141811.
63. Li Y−N, Chen Z−Y, Bao S−J, Wang M−Q, Song C−L, Pu S, et al. Ultrafine TiO_2 encapsulated in nitrogen−doped porous carbon framework for photocatalytic degradation of ammonia gas. *Chem. Eng. J.* **2018**, *331*, 383–388.
64. Shu Y, Ji J, Zhou M, Liang S, Xie Q, Li S, et al. Selective photocatalytic oxidation of gaseous ammonia at ppb level over Pt and F modified TiO_2. *Appl. Catal. B* **2022**, *300*, 120688.
65. Chen M, Zhang C, He H. Insights into Designing Photocatalysts for Gaseous Ammonia Oxidation under Visible Light. *Environ. Sci. Technol.* **2020**, *54*, 10544–10550.
66. Bühlmeyer H, Adamsen KC, Xu T, Lammich L, Libuda J, Lauritsen JV, et al. Adsorption and Reaction of NH_3 on Rutile TiO_2 (110): An STM Study. *J. Phys. Chem. C* **2022**, *126*, 6590–6600.
67. Yamazoe S, Teramura K, Hitomi Y, Shishido T, Tanaka T. Visible Light Absorbed NH_2 Species Derived from NH_3 Adsorbed on TiO_2 for Photoassisted Selective Catalytic Reduction. *J. Phys. Chem. C* **2007**, *111*, 14189–14197.
68. Yamazoe S, Okumura T, Hitomi Y, Shishido T, Tanaka T. Mechanism of Photo-Oxidation of NH_3 over TiO_2: Fourier Transform Infrared Study of the Intermediate Species. *J. Phys. Chem. C* **2007**, *111*, 11077–11085.
69. Yamazoe S, Hitomi Y, Shishido T, Tanaka T. Kinetic study of photo-oxidation of NH_3 over TiO_2. *Appl. Catal. B* **2008**, *82*, 67–76.
70. Kolinko PA, Kozlov DV. Products distribution during the gas phase photocatalytic oxidation of ammonia over the various titania based photocatalysts. *Appl. Catal. B* **2009**, *90*, 126–131.
71. Chen G, He P, Liu C, Mo X-F, Wei J-J, Chen Z-W, et al. Direct synthesis of hydrazine by efficient electrochemical ruthenium-catalysed ammonia oxidation. *Nat. Catal.* **2023**, *6*, 949–958.
72. Utsunomiya A, Okemoto A, Nishino Y, Kitagawa K, Kobayashi H, Taniya K, et al. Mechanistic study of reaction mechanism on ammonia photodecomposition over Ni/TiO_2 photocatalysts. *Appl. Catal. B* **2017**, *206*, 378–383.
73. Kebede MA, Varner ME, Scharko NK, Gerber RB, Raff JD. Photooxidation of Ammonia on TiO_2 as a Source of NO and NO_2 under Atmospheric Conditions. *J. Am. Chem. Soc.* **2013**, *135*, 8606–8615.
74. Kebede MA, Scharko NK, Appelt LE, Raff JD. Formation of Nitrous Acid during Ammonia Photooxidation on TiO_2 under Atmospherically Relevant Conditions. *J. Am. Chem. Soc.* **2013**, *4*, 2618–2623.
75. Zhou Y, Feng Y, Xie H, Lu J, Ding D, Rong S. Cryptomelane nanowires for highly selective self-heating photothermal synergistic catalytic oxidation of gaseous ammonia. *Appl. Catal. B* **2023**, *331*, 122668.
76. Wu H-L, Qi M-Y, Tang Z-R, Xu Y-J. Semiconductor quantum dots: A versatile platform for photoredox organic transformation. *J. Mater. Chem. A* **2023**, *11*, 3262–3280.
77. Li S-H, Qi M-Y, Tang Z-R, Xu Y-J. Nanostructured metal phosphides: From controllable synthesis to sustainable catalysis. *Chem. Soc. Rev.* **2021**, *50*, 7539–7586.